

Low-energy scales and temperature-dependent photoemission of heavy fermions

T. A. Costi

European Synchrotron Radiation Facility, BP 220, F-38043 Grenoble Cedex, France

N. Manini

*Dipartimento di Fisica, Università di Milano, Via Celoria 16 - 20133 Milano - Italy
and INFN, Unità di Milano, Milano, Italy*

We solve the $S = 1/2$ Kondo lattice model within the dynamical mean field theory. Detailed predictions are made for the dependence of the lattice Kondo resonance and the conduction electron spectral density on temperature and band filling n_c . Two low-energy scales are identified in the spectra: a renormalized hybridization pseudogap scale T^* , which correlates with the single-ion Kondo scale, and a lattice Kondo scale $T_0 < T^*$, which acts as the Fermi-liquid coherence scale. The lattice Kondo resonance is split into a main branch, which is pinned at the Fermi level, and whose width is set by T_0 , and an upper branch at $\omega \approx T^*$. The weight of the upper branch decreases rapidly away from $n_c = 1$ and vanishes for $n_c \lesssim 0.7$. In contrast, the pseudogap in the conduction electron spectral density persists for all n_c . On increasing temperature, the lattice Kondo resonance at the Fermi level vanishes on a temperature scale of order $10 T_0$, as in impurity model calculations. In contrast to impurity model spectra, however, the position of the lattice Kondo resonance depends strongly on temperature, particularly close to the Kondo insulating state. The results are used to make predictions on the temperature dependence of the low-energy photoemission and inverse photoemission spectra of metallic heavy fermions and doped Kondo insulators. We compare our results with available high-resolution measurements on YbInCu_4 and YbAgCu_4 . The loss in intensity with increasing temperature, and the asymmetric lineshape of the low-energy spectra are well accounted for by our model. More detailed agreement with experiment would require including the f -orbital degeneracy and crystal-field excited states.

PACS numbers: 75.30.Mb, 71.27.+a, 75.20.Hr, 79.60.-i

I. INTRODUCTION

Heavy fermions exhibit a number of interesting ground states with anomalous low-temperature properties [1–6]. These include paramagnetic heavy-fermion states down to the lowest temperatures (e.g. CeCu_6 , CeAl_3 , CeRu_2Si_2 , YbAgCu_4 , and YbInCu_4), magnetically ordered states with small ordering temperatures and reduced moments (e.g. URu_2Si_2 , CeAl_2), and unconventional superconducting states (e.g. CeCu_2Si_2 , UPt_3 , UPt_3). This anomalous behavior is mostly attributed to the strong correlations between the electrons in the localized or weakly-itinerant f states of the rare-earth (or actinide) ions. The natural starting point for understanding this peculiar behavior is the periodic Anderson model or, when charge fluctuations are negligible, its low-energy counterpart, the Kondo lattice model. These models are fairly well understood in one dimension where extensive calculations, based on exact diagonalization [7] and density matrix renormalization group [8] techniques are available. However, it is not clear how much of the insight gained is relevant to real-life three-dimensional heavy fermions. The Gutzwiller approximation, that can be applied in any dimension, has yielded some infor-

mation on various correlated lattice models [9], particularly for ground-state properties. The development of a non-perturbative approximation scheme, the dynamical mean field theory (DMFT) [10–14], has recently enabled a more comprehensive investigation of correlated lattice models, and particularly of their dynamic properties [15]. In this paper, we apply this technique to the Kondo lattice model in order to investigate (i) the relevant low-energy scales of the model and how these appear in the single-particle and magnetic excitation spectra, and (ii) the temperature dependence of the f -electron spectra for the interpretation of the low-energy photoemission spectra (PES) of paramagnetic heavy-fermion compounds, of current experimental interest [16–18].

The f -level photoemission and inverse photoemission spectra (IPES) of heavy fermions measure, respectively, the single-particle removal and addition spectrum for f electrons. They provide information on the electronic structure of heavy fermions, including the energies of the relevant f -level configurations, their spin-orbit splittings, and the size of the screened Coulomb interaction between the f electrons. In addition to this information about the “high-energy” scales (the smallest of these being the spin-orbit splitting ~ 1 eV), the f -level spectrum contains also information about low-energy scales associated with correlations and lattice coherence. Identifying these is one of the aims of the present study of the Kondo lattice model.

We shall not deal, here, with the “high-energy” part of

the spectra of heavy fermions, which is well accounted for by an Anderson impurity model (AIM) approach [19–21]. Instead, we shall focus our attention on the low-energy spectrum, which is the part most strongly influenced by lattice coherence effects, especially at low temperatures. These effects should emerge most clearly in the Kondo lattice model, which addresses specifically the low-energy scale, neglecting the complications associated with the high-energy atomic-like features. Although single-impurity model approaches also make predictions for the low-energy spectrum, there is no a priori reason to expect these to be quantitatively or even qualitatively correct. A lattice model calculation is therefore required to quantify the extent to which AIM calculations apply.

In the absence of detailed lattice-model calculations, the experimental results for the low-energy spectra of heavy fermions have, nevertheless, been discussed within the AIM approach. Two specific predictions of this approach concern the magnitude of the temperature dependence of the near- E_F feature (Kondo resonance) in the spectra, and the scaling of the intensity of this feature with the Kondo scale. Broad agreement with AIM predictions is claimed by some groups [18,22–25] whereas others [17,26,27] dispute the interpretation in terms of the AIM. The reader is referred to the reviews Ref. [17,18], and to Ref. [28–31], for some recent aspects of this controversy. In the context of this discussion, these experiments address a very important issue, namely the temperature dependence of the low-energy spectra and the appropriate theoretical framework for interpreting them. We shall attempt to clarify this issue by calculating the temperature dependence of the lattice Kondo resonance and comparing this with the predictions of the impurity models and with experimental spectra. Experimental studies of this temperature dependence at temperatures both above and below the relevant Kondo scale are technically difficult, and so far have only been carried out on a few systems, for example on YbAgCu₄ [23], YbAl₃ [24], and more recently on YbInCu₄ [31] and URu₂Si₂ [32]. Most other studies have only compared spectra at two temperatures, typically room temperature and at one low temperature comparable to the Kondo scale: this is not sufficient for an unambiguous testing of model predictions with experiment, but can at most indicate agreement with predicted trends. Hence, it is important for a detailed comparison with theory for more experiments of the former type to be carried out.

This paper is organized as follows: in Sect. II we introduce the quantities of interest for the Kondo lattice model, and sketch the dynamical mean field method used; in Sect. III we discuss the main theoretical findings; in Sect. IV we describe the results for the PES and IPES intensities; Sect. V contains the comparison of the theoretical spectra with actual PES data for YbInCu₄ and YbAgCu₄; Sect. VI summarizes the main findings and problems left open by this paper; Appendix A provides

details on the implementation of the DMFT to the Kondo lattice model and an expression for the self energy; Appendix B defines the relevant spectral functions for this study.

II. THE KONDO LATTICE MODEL AND THE DMFT METHOD

A. The Kondo lattice model

Consider the Kondo lattice model, given by the Hamiltonian

$$\mathcal{H} = \sum_{\mathbf{k},\sigma} \epsilon_{\mathbf{k}} c_{\mathbf{k},\sigma}^\dagger c_{\mathbf{k},\sigma} + \sum_j J \mathbf{S}_j \cdot \mathbf{s}_j . \quad (1)$$

The first term in the above represents non-interacting itinerant electrons with dispersion relation $\epsilon_{\mathbf{k}}$. The second term is the antiferromagnetic exchange interaction, of strength J , between the localized spins \mathbf{S}_j at lattice sites j and the local conduction electron spin density $\mathbf{s}_j = \sum_{\mu,\nu} c_{j,\mu}^\dagger \boldsymbol{\sigma}_{\mu\nu} c_{j,\nu}$, where $c_{j,\sigma} = N_{\text{sites}}^{-1/2} \sum_{\mathbf{k}} c_{\mathbf{k},\sigma} \exp(i\mathbf{k} \cdot \mathbf{R}_j)$ destroys a local conduction electron orbital at site j . This model is relevant for heavy fermions with negligible charge fluctuations on the f orbitals: it is appropriate for describing Ce and Yb compounds having a doublet crystal-field ground state for the $4f^1$ (Ce) or $4f^{13}$ (Yb) atomic configuration, acting as a $S = 1/2$ pseudospin represented in the model by the \mathbf{S}_j operator.

For the unperturbed density of states of the lattice, $\rho_0(\omega)$, we take a semi-elliptic form

$$\rho_0(\omega) = \sum_{\mathbf{k}} \delta(\omega - \epsilon_{\mathbf{k}}) = \frac{2}{\pi D^2} \sqrt{D^2 - \omega^2} , \quad (2)$$

corresponding to a Bethe lattice. The main features of the local dynamical quantities discussed below are primarily a result of the correlations and not of this particular choice of lattice, which is especially convenient in the DMFT.

B. DMFT and numerical renormalization group

To treat the complicated correlation problem expressed by Eq. (1) we resort to a standard technique developed in the context of the infinite dimensional limit of correlated lattice models [10], the DMFT [15]. In the DMFT approximation, the solution of (1) reduces to solving a quantum impurity model embedded in an effective conduction electron medium, whose spectral density $\tilde{\rho}(\omega) = \sum_{\mathbf{k}} \delta(\omega - \tilde{\epsilon}_{\mathbf{k}})$ is determined self-consistently [12–14]. In the present case of the Kondo lattice model, the effective quantum impurity model is just the $S = 1/2$ Kondo model [33]

$$\mathcal{H}_{imp} = \sum_{\mathbf{k},\sigma} \tilde{\epsilon}_{\mathbf{k}} c_{\mathbf{k},\sigma}^\dagger c_{\mathbf{k},\sigma} + J \mathbf{S} \cdot \mathbf{s}, \quad (3)$$

where \mathbf{S} is the impurity spin and \mathbf{s} is the spin density of the conduction electrons at the impurity site. The effective medium is determined from the self-consistency requirement that the local conduction-electron Green's function of the effective impurity model $G_c(\omega, T)$ (which depends implicitly on $\tilde{\epsilon}_{\mathbf{k}}$) be identical to the local lattice Green's function $G_L(\omega, T)$, i.e.

$$G_{c,\sigma}(\omega, T) = G_{L,\sigma}(\omega, T) \equiv \sum_{\mathbf{k}} \frac{1}{\omega + \mu - \epsilon_{\mathbf{k}} - \Sigma_\sigma(\omega, T)}. \quad (4)$$

Here, $\Sigma_\sigma(\omega, T)$ is the conduction-electron self energy, which is independent of \mathbf{k} due to the local nature of the DMFT approximation [11]. In the following we drop spin indices for the Green's functions and the self energy since, in this paper, we shall only be interested in paramagnetic solutions of the Kondo lattice model.

To solve the effective single-impurity problem (3) we use Wilson's numerical renormalization group (NRG) [34] extended to finite-temperature spectra [35,36], which is based on a logarithmic discretization that allows the low-energy scales (such as the Kondo resonance) to be accessed with high resolution. The self-consistency procedure involves: (i) guessing an initial form for the effective medium $\tilde{\rho}(\omega) = \sum_{\mathbf{k}} \delta(\omega - \tilde{\epsilon}_{\mathbf{k}})$, (ii) diagonalizing (3) with the NRG and solving for its dynamics, (iii) re-calculating the effective medium by using Eq. (4). Steps (ii)-(iii) are repeated until self-consistency is reached. Further details of the NRG and the DMFT procedure, which we refer to as DMFT(NRG), are given in Appendix A. For an application of the DMFT(NRG) to the finite-temperature Mott transition in the Hubbard model see Ref. [37].

In addition to the condition (4) on the Green's functions, we also fix the number of electrons n_c in the conduction band, by adjusting the chemical potential μ at each iteration, until n_c converges to the desired value. This number is obtained in terms of the local conduction electron density of states $\rho_c(\omega, T)$, as

$$n_c = N_{\text{sites}}^{-1} \sum_{j,\sigma} \langle c_{j,\sigma}^\dagger c_{j,\sigma} \rangle = \int_{-\infty}^{+\infty} d\omega f_T(\omega) \rho_c(\omega, T), \quad (5)$$

where $f_T(\omega) = 1/(1 + \exp[(\omega - \mu)/T])$ is the Fermi function (the Boltzmann constant and \hbar are taken to be unity throughout the paper). The interacting conduction electron density of states, in turn, is defined by

$$\rho_c(\omega, T) = -\frac{1}{\pi} \text{Im} G_c(\omega, T). \quad (6)$$

The chemical potential self-consistency is not implemented in impurity-model calculations, but it is

clearly required for concentrated systems, such as heavy fermions.

The quantity of main interest in this paper is the f -electron PES $A(\omega, T)$. This is defined in Appendix B together with another useful quantity we shall consider: $\chi''_{zz}(\omega, T)$, the spectral density of magnetic excitations for the effective quantum impurity model.

C. The role of the band-filling n_c

We now discuss the significance of the other parameter in the Kondo lattice model: the band filling n_c . The $c_{\mathbf{k},\sigma}^\dagger$ fermions represent renormalized Bloch states in the wide metallic bands of the crystal, with the correct symmetry for coupling to the localized f states. Even in a stoichiometric compound, with integer number of electrons per unit cell, the effective occupancy of the c band need not be commensurate, since the conduction electrons are shared between the c band and other bands of different symmetry, not included in the model. Thus, $n_c = 1$ represents the special case of particle-hole symmetry in this effective band: it is appropriate for Kondo insulators (examples of which include $\text{Ce}_3\text{Bi}_4\text{Pt}_3$, SmB_6 , YbB_{12} , CeNiSn , and SmS [38]), since ρ_c , A and χ''_{zz} show true gaps at $T = 0$. $n_c \neq 1$ addresses naturally incommensurate filling of this effective band. In particular, $n_c \approx 1$ can be realized by doping the Kondo insulators, e.g. by substitution of Ce with La in $\text{Ce}_3\text{Bi}_4\text{Pt}_3$ [39] or of Yb with Lu in YbB_{12} [40]. Intermediate values of $n_c \approx 0.5$ describe metallic heavy fermions, which we study in detail in Sect. V. Finally, small values of n_c should be relevant to low carrier-density heavy-fermion systems, e.g. Yb_4As_3 and YbBiPt [41].

In addition to this direct significance of n_c representing the actual number of electrons coupled to the f states in different materials, one can also attach a second meaning to a variable n_c : deviations of n_c away from unity introduce particle-hole asymmetry into the model. Such an asymmetry is generally present in the Anderson lattice model and results from an asymmetric position of the f level with respect to E_F . In the Kondo lattice model, the f level is projected out and real charge fluctuations are absent ($n_f \equiv 1$). Although there is no f level in the latter, one can still partly simulate the effects of different f -level positions by changing instead the Fermi-level position E_F , i.e. by varying n_c . Within this scheme, Ce heavy-fermion compounds correspond to $n_f + n_c \leq 2$, i.e. $0 < n_c < 1$, and Yb compounds are the particle-hole counterparts of these with $1 < n_c < 2$. Here, we only compute spectra in the range $0 < n_c < 1$, relevant for the spectroscopy of Ce systems: the complementary region $1 < n_c < 2$, relevant for Yb systems, is obtained by particle-hole symmetry exchanging $\omega \rightarrow -\omega$ in the spectral functions.

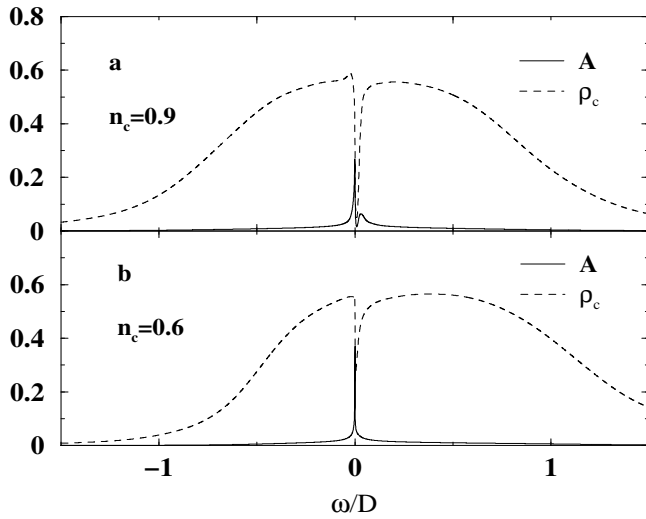


FIG. 1. The spectral density $A(\omega, T = 0)$ of the lattice Kondo resonance (solid line) and of the conduction electrons $\rho_c(\omega, T = 0)$ (dashed line), for (a) $n_c = 0.9$, and (b) $n_c = 0.6$. The detailed behavior near the Fermi level is shown in Fig. 2.

III. RESULTS

All calculations are carried out for $J/D = 0.3$, sufficiently smaller than unity for the low-energy spectra to show universal scaling with the Kondo-energy scale, but also sufficiently large to avoid unnecessarily large numbers of NRG iterations in the region of small band filling, where the Kondo scale becomes very small. All spectra are measured with frequency ω relative to the chemical potential μ .

A. $T = 0$ spectral densities and low-energy scales

Figure 1 shows the zero-temperature spectra for ρ_c and A on a wide energy scale, of the order of the unperturbed bandwidth $W = 2D$, and for two fillings, $n_c = 0.9$ and $n_c = 0.6$. The large-scale effects of interaction on ρ_c are clearly visible: band spreading, the opening of a renormalized hybridization pseudogap and consequently a reduction in height of the conduction electron spectral density relative to the unperturbed spectral density (2). These global effects, on the scale of the whole band depend on the particular value of J and n_c : we are interested instead in the low-energy behavior of the spectral functions, which, instead, is universal, i.e. independent of J (but depend on n_c).

Figure 2 zooms close to the Fermi level on the $T = 0$ spectra, plotting them for different band fillings n_c . Two different energy scales emerge clearly in these spectra.

As soon as n_c moves away from 1 (Fig. 2a), the $n_c = 1$ insulating gap turns into a *pseudogap*, for all spectra. We denote the characteristic width of this pseudogap in ρ_c

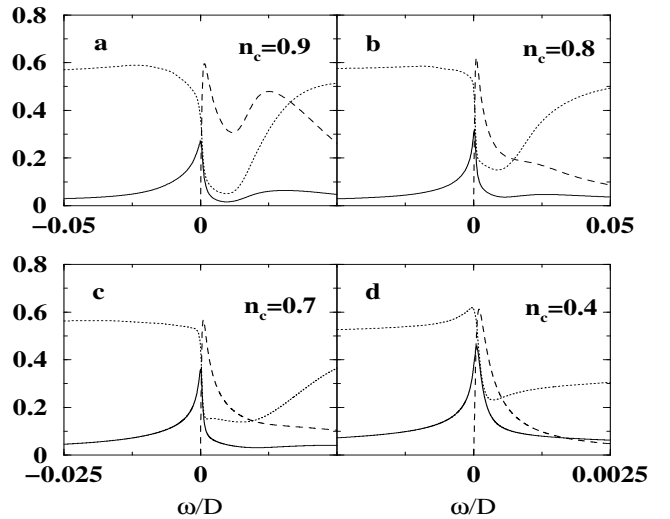


FIG. 2. The $T = 0$ conduction electron spectral density $\rho_c(\omega, 0)$ (dotted line), the lattice Kondo resonance $A(\omega, 0)$ (solid line), and the magnetic excitation spectrum $\chi''_{zz}(\omega, 0)$ (dashed line), for decreasing band fillings: (a) $n_c = 0.9$, (b) $n_c = 0.8$, (c) $n_c = 0.7$, and (d) $n_c = 0.4$. The curves for χ'' are rescaled arbitrarily for the purpose of comparison with ρ_c and A . Different frequency ranges are used in (a-d), as the lattice Kondo scale is decreasing with decreasing n_c (see text).

by T^* . The pseudogap in ρ_c lies just above the Fermi level for $n_c < 1$ (and, by particle-hole symmetry, just below the Fermi level for $n_c > 1$). It persists for all n_c , but becomes increasingly asymmetrical and step-like as $n_c \rightarrow 0$ (see Fig. 2b-d), making its precise value increasingly more difficult to specify accurately. Consequently, we have not made an exhaustive analysis of the dependence of T^* on n_c , but our calculations in the range $0.2 \lesssim n_c \lesssim 0.96$ indicate that T^* decreases slowly with decreasing n_c and that it correlates approximately with the single-ion Kondo scale, being a factor of 2 – 3 larger than this, if we define the latter as the full width at half maximum (FWHM) of the single-ion Kondo resonance at $T = 0$. We find $T^*/D \approx 0.02 - 0.025$ for $n_c \gtrsim 0.6$. The pseudogap in A manifests itself for n_c close to 1. The A -spectrum represents the lattice Kondo resonance split by hybridization effects into a lower branch pinned at the Fermi level and an upper branch at $\omega \approx T^*$. The upper branch loses intensity at the expense of the main branch at the Fermi level with decreasing n_c , and it eventually disappears for $n_c \lesssim 0.7$. Our conclusion is that in the $S = 1/2$ Kondo lattice model, a splitting of the Kondo resonance by hybridization effects is only discernible close to half-filling ($n_c \gtrsim 0.7$), although in principle such a splitting is present for all n_c (see Ref. [42,43]). The pseudogap is present also in the spectrum of the magnetic excitations χ''_{zz} : a peak at $\omega \approx T^*$ for n_c close to half-filling represents excitations across a spin pseudogap. On decreasing n_c , the peak in χ''_{zz} at $\omega \approx T^*$ becomes a shoulder

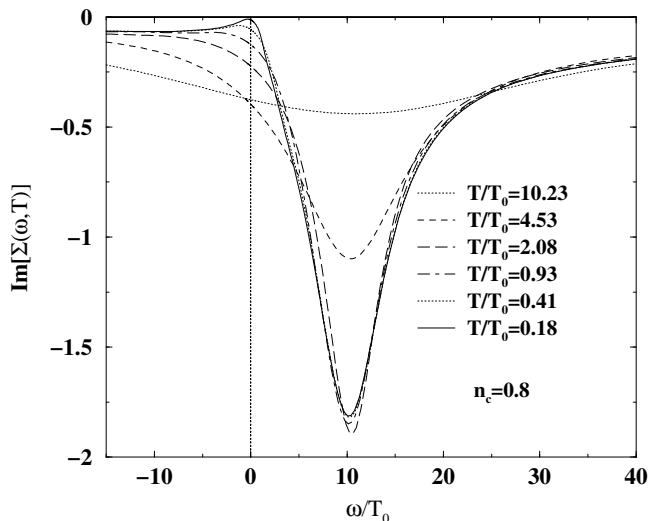


FIG. 3. Temperature dependence of the imaginary part of the self-energy $\text{Im}[\Sigma(\omega, T)]$ for $n_c = 0.8$, showing that T_0 [44] is the Fermi liquid coherence scale.

der at $n_c = 0.8$, and then it disappears for $n_c \lesssim 0.7$, together with the upper branch of the lattice Kondo resonance in A . In contrast, for ρ_c the pseudogap persists for all n_c , so that T^* remains a relevant scale for this quantity at all band fillings.

The second energy scale apparent in the spectra of Fig. 2 is associated with the onset of Fermi-liquid coherence (as will become clearer with the discussion of the self energy below). It appears in Fig. 2 as the characteristic width of the $T = 0$ lattice Kondo resonance in A (i.e. its main branch at the Fermi level), the lowest peak in the magnetic excitation spectrum χ''_{zz} and also as the energy range over which ρ_c has a drop at the Fermi level. Clearly, there are several ways of defining this scale T_0 . In this paper we define it as the position of the lowest-energy peak in the $T = 0$ magnetic excitation spectrum χ''_{zz} . The Kondo scale T_0 , defined in this way, has the same dependence on n_c and J as that defined in other ways, but may differ from these by factors of order unity (for example, the scale T_K defined as one half of the FWHM of the Kondo lattice resonance is 2-3 times larger than T_0). We have compared the dependence of T_0 on n_c [44] with that of the single-ion Kondo scale, T_{imp} (defined in the same way as T_0 , i.e., as the low-energy peak position in the local dynamical susceptibility, and using the same J and ρ_0 as for the lattice model calculations). For $n_c \geq 0.4$, T_0/T_{imp} is consistent with the form $n_c \exp(p n_c)$, with $p \approx 5/2$, found for the Anderson lattice model in the strong-correlation Kondo limit [45] within the DMFT(NRG) approach. Burdin *et al.* [46], using a slave-boson mean field approach, also find an increase of T_0/T_{imp} with n_c .

The relative magnitude of the two energy scales T^* and T_0 , is determined by both J and n_c . We find that,

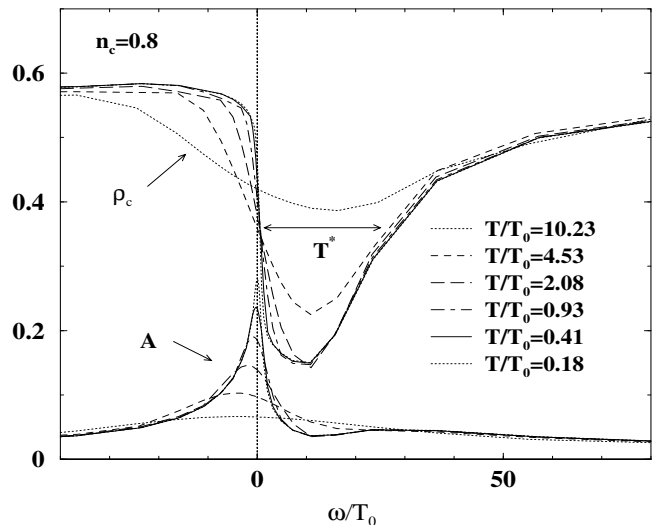


FIG. 4. Temperature dependence of ρ_c for $n_c = 0.8$ in the region near the Fermi level and the pseudogap. The A -spectrum is shown for comparison. Temperatures and energies are shown in units of T_0 [44].

for fixed n_c , both T_0 and T^* have the same J -dependent renormalization with decreasing J . T_0 and T^* are closest near half-filling and become increasingly differentiated with decreasing n_c (see also Fig. 4-5 below).

B. T dependence of the self-energy

Figure 3 shows the temperature and frequency dependence of the imaginary part of the conduction electron self-energy $\text{Im}[\Sigma(\omega, T)]$. It vanishes at low temperatures at $\omega = E_F$ on a temperature scale of order T_0 . This is consistent with the interpretation of T_0 as the Fermi-liquid coherence scale. The strong damping close to $\omega \sim T^*$ is associated with incoherent excitations due to the pseudogap in ρ_c . It correlates with the position of the broad high-energy peak in the magnetic excitation spectrum of Fig. 2b.

C. T dependence of ρ_c and χ''_{zz}

The role of the two energy scales T^* and T_0 in the spectra is further clarified in Fig. 4-5 which show the temperature dependence of ρ_c for $n_c = 0.8$ ($T^*/T_0 \approx 17$) and $n_c = 0.4$ ($T^*/T_0 \approx 300$). The temperature dependence of A is shown for comparison and will be discussed in detail below. We see that, as for the self-energy, the Fermi-liquid scale T_0 also sets the scale for the temperature dependence of ρ_c close to the Fermi level (just as for A). The feature of the ρ_c spectrum directly affected on this temperature scale is the sharp drop at E_F . Instead, the region near the minimum of the pseudogap in ρ_c (and, whenever it exists, also in A and χ''_{zz}) starts to

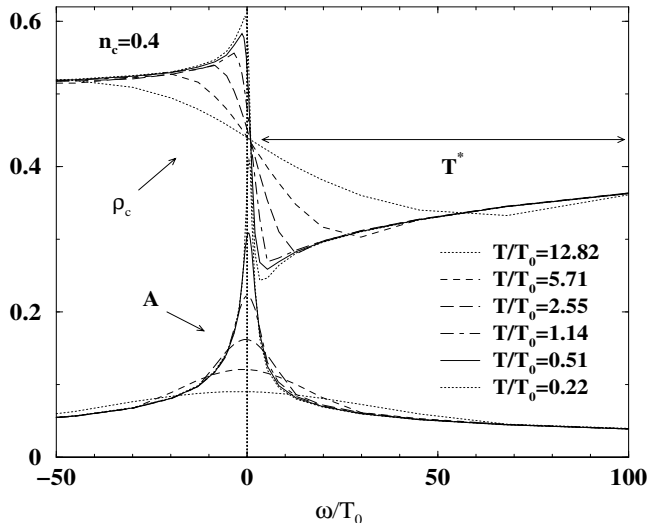


FIG. 5. Temperature dependence of ρ_c for $n_c = 0.4$ in the region near the Fermi level and the pseudogap. The A -spectrum is shown for comparison.

evolve at temperatures larger than T_0 . It finally closes at higher temperatures $T \gtrsim T^*$.

For band fillings $n_c \gtrsim 0.7$, the pseudogap is also evident in χ''_{zz} . Figure 6 shows that T_0 sets the scale for the temperature dependence of a quasielastic peak, whereas excitations across a spin pseudogap (of order T^*) give rise to a peak in χ''_{zz} at $\omega \sim T^*$. The temperature dependence of the latter is set by the scale T^* . This type of response also characterizes the Kondo insulating behavior at $n_c = 1$, as long as $T > 0$, so that the gap behaves effectively as a pseudogap at finite temperature, as seems typical of correlated insulators [47]. The neutron scattering results for CeNiSn [48] and Ce₃Bi₄Pt₃ [49] show qualitatively the same temperature dependence.

D. Discussion of the two energy scales

At high temperatures, approaching the scale T^* , the spectra are similar to those of a Kondo impurity, namely the split Kondo resonance in A for $n_c \geq 0.7$ reverts to a single-ion like Kondo resonance at the Fermi level whose height decreases with increasing temperature (see Fig. 7a), χ''_{zz} has a peak at $\omega \approx T^*$ whose height also decreases with increasing temperature, and ρ_c is approximately independent of temperature. The physics appears like that of a collection of quasi-independent Kondo scatterers, since T^* correlates with the single-ion Kondo scale describing the high-temperature properties of these Kondo scatterers. On decreasing the temperature, the effects of lattice coherence become quite pronounced for $T \approx T^*$: the spectra develop a pseudogap resulting from the formation of hybridized bands between the f and conduction states. Fermi-liquid coherence only sets in at much lower temperatures, specifically for $T \ll T_0$. The

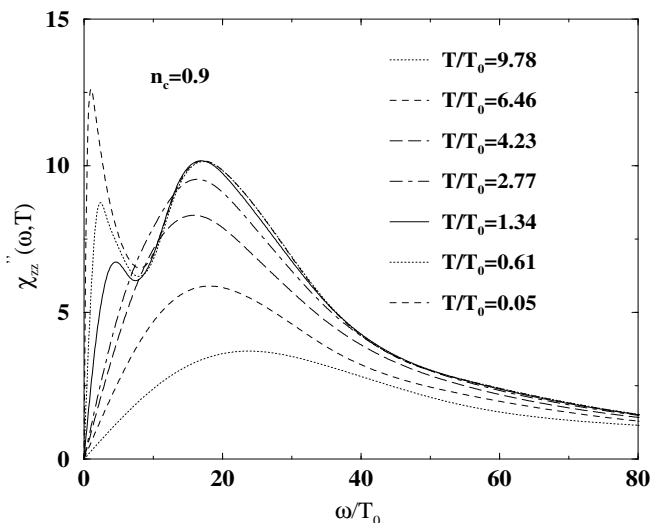


FIG. 6. Temperature dependence of χ''_{zz} for $n_c = 0.9$. This type of response is similar to the Kondo insulating behavior measured for CeNiSn [48] and Ce₃Bi₄Pt₃ [49].

formation of the paramagnetic heavy-fermion state therefore appears to proceed in two stages: a single-ion Kondo effect at $T \gg T^*$ involving essentially non-interacting conduction electrons, and a low-temperature Kondo effect at $T < T^*$ involving also the f electrons and leading to a reduced lattice Kondo scale T_0 describing just the width of the main branch of the split Kondo resonance at the Fermi level. Two energy scales, a single-ion and lattice Fermi-liquid Kondo scale, have also been found within a recent slave-boson treatment of the Kondo lattice model [46].

E. T dependence of the Kondo resonance

Figure 7 shows the temperature dependence of the lattice Kondo resonance for several band fillings. Compare the behavior of the main branch of the lattice Kondo resonance away from half filling with that calculated within the AIM [35], and shown in Fig. 8. The lattice Kondo resonance, like the impurity one, is pinned to just above the Fermi level for $T \ll T_0$. However, in contrast to the impurity case, the peak position $E_m(T)$ relative to the chemical potential *shifts to below* the Fermi level on a scale $\lesssim T_0$ with increasing temperature. This effect is particularly evident slightly away from half-filling (e.g. $n_c = 0.9$ in Fig. 7a), and it becomes less pronounced as the band filling decreases toward zero, but is still significant as compared to the impurity-model predictions (Fig. 8). For the band fillings shown in Fig. 7, $n_c \geq 0.4$, the lattice Kondo resonance vanishes on a scale of approximately $10 T_0$. This is the same scale over which the single-impurity Kondo resonance vanishes (see Fig. 8). We therefore do not see a significantly slower dependence

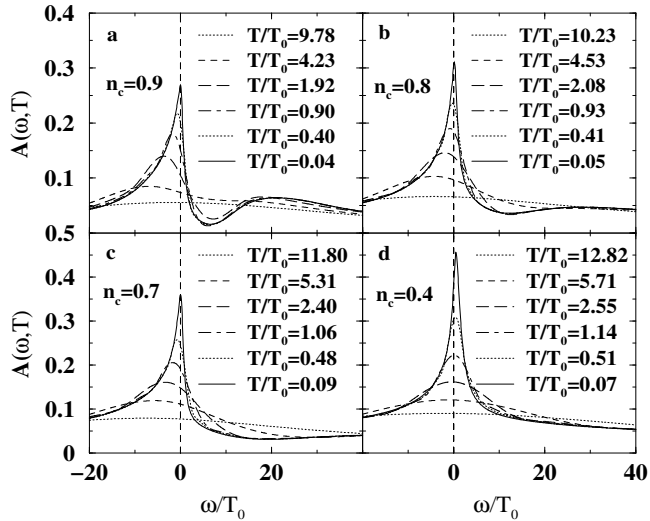


FIG. 7. Temperature dependence of the lattice Kondo resonance for the same band fillings as in Fig. 2. Temperatures and energies are shown in units of T_0 , where T_0 is the lattice Kondo scale appropriate for each n_c and defined in the text [44].

(termed “protracted behavior” [50]) of the height of the lattice Kondo resonance as compared to the impurity one. This contradicts the $n_c = 0.4$ PES calculations for the periodic Anderson model of Ref [51]. Our calculations cannot rule out, however, that such “protracted” behavior might be present in other quantities, such as in the static susceptibility, or that such behavior will appear in spectral densities for $n_c \ll 1$ (the “exhaustion” limit [52], an important conceptual limit that shall require clarification: we have not addressed this here, because we are mainly interested in metallic heavy fermions with appreciable band fillings). For a recent experimental evaluation of the “protracted screening” scenario see Ref. [53].

IV. T DEPENDENCE OF PES AND IPES

The low-energy PES (I_-) and IPES (I_+) intensities are defined by

$$I_-(\omega, T) = f_T(\omega)A(\omega, T) \quad (7)$$

$$I_+(\omega, T) = (1 - f_T(\omega))A(\omega, T). \quad (8)$$

For comparison with the Kondo lattice model predictions, we first outline the PES and IPES spectra from the AIM.

A. T dependence of PES and IPES for the AIM

A typical T -dependent Kondo resonance from the AIM is shown in Fig. 8. The derived PES and IPES are shown in Fig. 9. It is often stated that the PES intensity in Ce

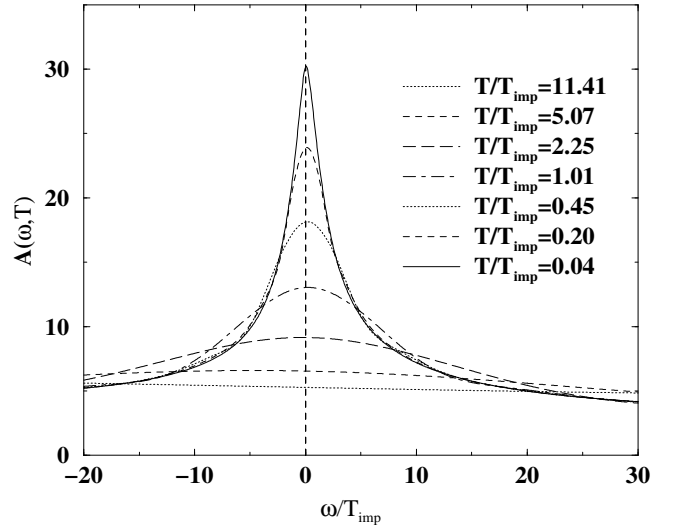


FIG. 8. Temperature dependence of the impurity Kondo resonance calculated from the AIM in the Kondo regime by using the NRG [35]. The local level position used is $\varepsilon_d = -4\Delta$ and the Coulomb interaction $U = 4\pi\Delta$, with $\Delta = 0.1D$ the hybridization strength and $D = 1$ the half-bandwidth for a flat conduction band $\rho_0(\omega) = 1/2D$. The Kondo scale, $T_{\text{imp}} = 4.22 \times 10^{-4}D$, is defined for the impurity model in the same way as for the lattice model, as the peak position in the $T = 0$ magnetic excitation spectrum.

compounds is very small compared to the IPES intensity because the Kondo resonance has most of its weight above the Fermi level. For the present $N = 2$ AIM we see that the Kondo resonance is, in fact, pinned very close to the Fermi level. Correspondingly, we observe nearly equal intensities in PES and IPES spectra in Fig. 9. This does not contradict many PES and IPES experiments on Ce compounds, however, since most of these experiments are carried out at temperatures and resolutions far above the typical energies of the crystal field excitations or Kondo scale. As a result, they probe the full $N = 6$ degeneracy of the Ce $4f^1$ configuration and therefore cannot be described within an AIM with $N = 2$. Including the orbital degeneracy in the AIM is known to shift the position of the Kondo resonance to further above the Fermi level [2], and therefore to increase the asymmetry between the PES and IPES intensities, as observed in many Ce (and Yb) heavy fermions. Nevertheless, in systems where the $N = 2$ AIM approach is applicable, the spectra of Fig. 9 suggest that experiments at sufficiently high resolution and low enough temperatures (such that only the low-energy doublet is effectively playing a role) should give nearly equal intensities in PES and IPES for a system with a doublet ground state.

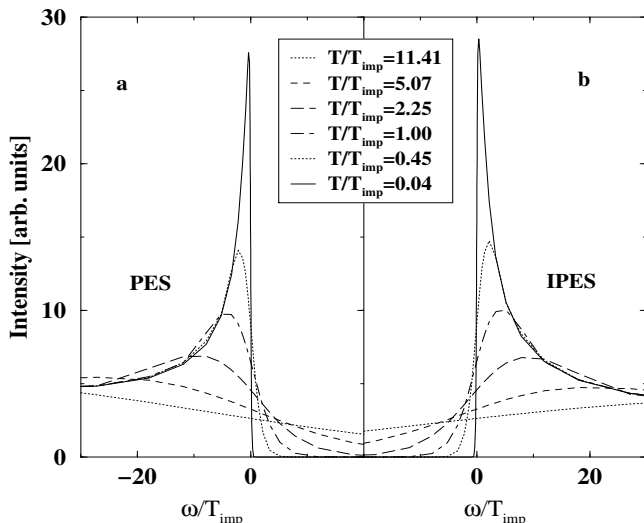


FIG. 9. Temperature dependence of the low-energy PES intensity (left) and IPES intensity (right) for the impurity Kondo resonance calculated from the AIM in the Kondo regime using the NRG [35]. The same temperatures as in Fig. 8 are used.

B. T dependence of PES and IPES for the Kondo lattice model

The PES and IPES intensities for the Kondo lattice model are more complicated and show a range of behaviors, depending on band filling n_c . Fig. 10-13 shows the PES and IPES intensities for the four band fillings $n_c = 0.9$, $n_c = 0.8$, $n_c = 0.7$ and $n_c = 0.4$ of Fig. 7.

For Kondo insulators ($n_c = 1$), there is experimental evidence on $\text{Ce}_3\text{Bi}_4\text{Pt}_3$ [54] and CeRhAs [55] indicating the development of a gap in the PES on decreasing temperature. This is consistent with our predictions for the A -spectrum at $n_c = 1$, to be published elsewhere, and also with calculations on the symmetric Anderson lattice model [47,56].

The results for n_c close to 1 (Fig. 10) are relevant to doped Kondo insulators, e.g. to hole-doped Ce systems, such as $\text{Ce}_{3-x}\text{La}_{1-x}\text{Bi}_4\text{Pt}_3$ [39]. As noted earlier (see Fig. 7), the Kondo resonance is highly asymmetric for $n_c \lesssim 1$ with most of its weight lying below the Fermi level. Consequently, the bulk of the intensity in Fig. 10 lies in the PES part of the spectrum. In addition the strong shift of the Kondo resonance from above to below the Fermi level on increasing temperature for the case $n_c \lesssim 1$, noted in Sect. III, further diminishes the near- E_F intensity in IPES as compared to that in the PES.

Another interesting feature of our calculations is that the pseudogap can be seen as a dip in the IPES intensity at $\omega \approx T^*$, which becomes increasingly well developed with decreasing temperature. Our predictions for hole-doped Ce systems apply equally well, by particle-hole symmetry, to electron-doped Yb systems. Results for the electron-doped Kondo insulator $\text{Yb}_{1-x}\text{Lu}_x\text{B}_{12}$ [57]

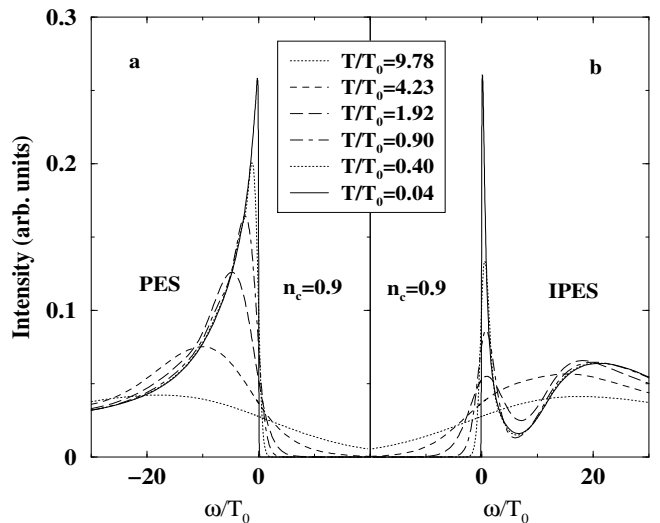


FIG. 10. Temperature dependence of the low-energy PES intensity (left) and IPES intensity (right) for the lattice Kondo resonance for $n_c = 0.9$ (rather close to the Kondo insulating case $n_c = 1$). The temperatures shown correspond to those in Fig. 7a.

indeed indicate an increase in the photoemission intensity at the Fermi level upon doping YbB_{12} with Lu.

On further decreasing the band filling (Fig. 11-13), the IPES intensity increases with respect to the PES intensity. This results from the more symmetric lattice Kondo resonance together with the tendency of this resonance to move further above the Fermi level for smaller n_c . In addition, the pseudogap in the IPES intensity fills in below $n_c \approx 0.7$. For $n_c = 0.4$, far enough from the Kondo insulating state to be representative of metallic heavy fermion systems, we find a behavior rather similar to the AIM spectra, i.e. the IPES intensity is slightly larger than the PES intensity at low temperatures, $T \ll T_0$. However, a small increase of the temperature to $T \gtrsim T_0$ makes these intensities nearly equal (e.g. Fig. 13). Inclusion of the orbital degeneracy of the f -level should lead to a displacement of the lattice Kondo resonance further above the Fermi level, as occurs in impurity models, and consequently to larger IPES intensities for Ce systems than PES intensities.

V. COMPARISON WITH EXPERIMENTS

Ideally, our predictions for the $S = 1/2$ Kondo lattice model are suitable for heavy-fermion systems with a local doublet ground state characterized by a separation Δ_{CF} from the first crystal-field excitation much larger than the Kondo scale T_0 . An example of such a system would be CeCu_2Si_2 , which has $T_0 \sim 6$ K and $\Delta_{\text{CF}} \sim 30$ meV [58]. Photoemission spectra have been measured for this compound [59] at 6 meV resolution (FWHM). The absolute resolution is high, but the relative resolution for

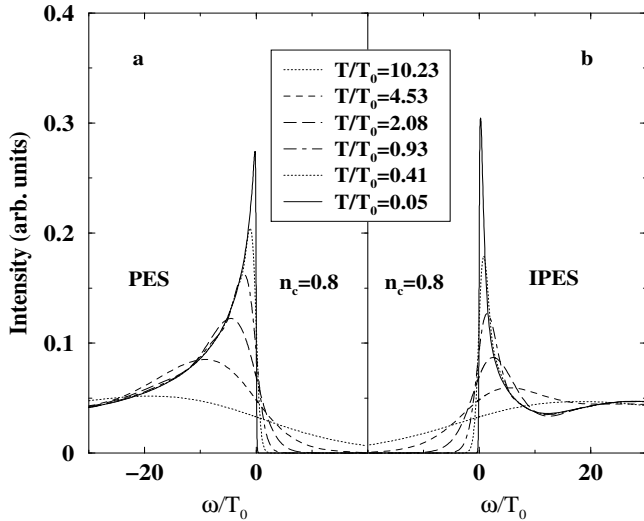


FIG. 11. Temperature dependence of the low-energy PES intensity (left) and IPES intensity (right) for the lattice Kondo resonance for $n_c = 0.8$. The temperatures are those of Fig. 7b.

probing the Kondo resonance is still quite low due to the small Kondo scale. Moreover, most measurements were taken at temperatures $T \gtrsim 10T_0$, with only one temperature ($T = 15$ K) relevant for testing predictions about the Kondo resonance. In this respect, the experiments on YbAgCu_4 [23] and YbInCu_4 [31] are more promising, since measurements were taken at T both above and below the relevant Kondo scales. Unfortunately, for these systems, neutron scattering studies [60,61] indicate that the crystal-field excitation energy is comparable to the Kondo scale ($\Delta_{\text{CF}} \sim T_0$). In the temperature range of the experiments $T \sim 10 - 200$ K, thermal population of the crystal-field states will be important and would require further refinements of our $S = 1/2$ model, which, however, are beyond the scope of the present work. With this proviso, we compare our results, which include lattice coherence and correlation effects, with measurements of the temperature dependence of the low-energy f -spectrum for YbInCu_4 [31] and YbAgCu_4 [23].

YbInCu_4 exhibits an isostructural phase transition, similar to that of Ce, with a 0.5% volume change and a 0.1 change in f -level occupancy at a temperature $T_v = 42$ K. Both phases show the characteristic features of paramagnetic heavy-fermion behavior. The high-temperature phase has a Kondo scale $T_0 = 30$ K, whereas the low-temperature phase has a much larger Kondo scale $T_0 = 400$ K [62]. Temperature-dependent photoemission measurements were carried out in both phases [31] ($T = 12-40$ K for the low-temperature phase, and $T = 50-150$ K for the high-temperature phase).

YbAgCu_4 shows a single paramagnetic heavy-fermion phase down to the lowest temperatures [63]. Neutron-scattering experiments indicate a quartet crystal-field

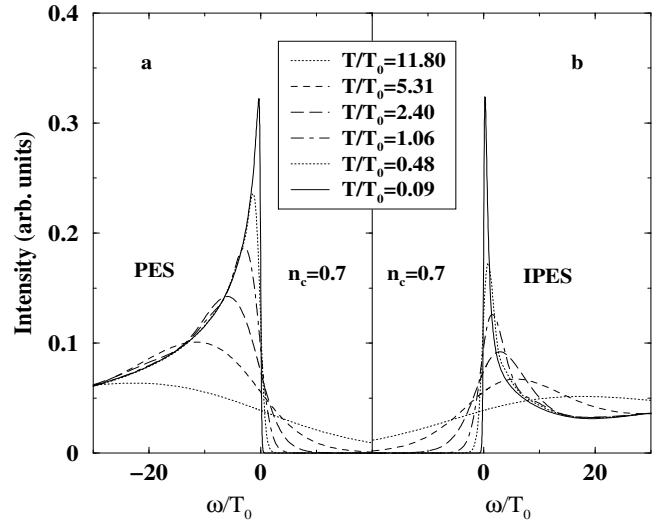


FIG. 12. Temperature dependence of the low-energy PES intensity (left) and IPES intensity (right) for the lattice Kondo resonance for $n_c = 0.7$. The temperatures are those of Fig. 7c.

ground state with a Kondo scale $T_0 = 100$ K [61], consistent with thermodynamic measurements [64]. Measurements for this compound were carried out in the temperature range 20–260 K and show a strong temperature dependence of the near- E_F feature in qualitative agreement with expectations from Kondo phenomenology [23].

The experiments on YbInCu_4 used single crystals in contrast to the polycrystals used for YbAgCu_4 . In both experiments, one observes a near- E_F feature (due to excitations from the $f^{7/2}$ ground state of the Yb ions), interpreted as the Kondo resonance, and an $f^{5/2}$ spin-orbit side band at approximately 1 eV below E_F . The bulk and surface contributions to these excitations can be separated in the experiments, allowing bulk effects to be investigated. The $f^{5/2}$ spin-orbit side-band is not included in our model, but its absence will not affect the overall predictions for the $f^{7/2}$ excitation in a range of $\ll 1$ eV around the E_F spectrum.

The experimental resolution ($\Delta E = 25$ meV FWHM) is included by convoluting the calculated intensities (described in Sect. IV) with the appropriate Gaussian broadening. Since the resolution is comparable to or below typical Debye energies, some effect of phonon broadening on the spectra may be observable [26,31]. Specifically, for both YbInCu_4 and YbAgCu_4 , we take a Gaussian phonon broadening term of the form $\Delta E_{ph} = \alpha T$ reaching 50 meV at 150 K [31]: the total width used to convolute the calculated intensities is then given by

$$\Delta E_{tot} = (\Delta E_{ph}^2 + \Delta E^2)^{1/2}. \quad (9)$$

For all the comparisons, we use an intermediate value $n_c = 0.4$. This choice is motivated by the requirement of being in a regime representative of metallic heavy

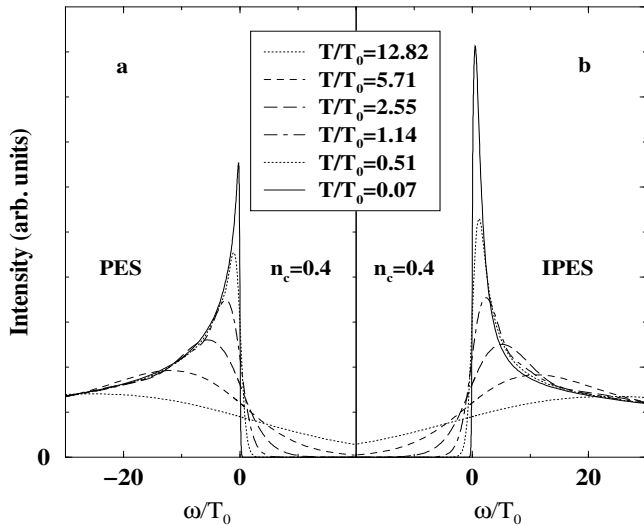


FIG. 13. Temperature dependence of the low-energy PES intensity (left) and IPES intensity (right), for the lattice Kondo resonance for $n_c = 0.4$. The temperatures are those of Fig. 7d.

fermions, characterized by an asymmetric position of the localized f states.

A. Low-temperature phase of YbInCu_4

In Fig. 14 we compare the calculated and experimental intensities for YbInCu_4 at the lowest temperature $T = 12$ K at which measurements were taken in the low-temperature phase (the curves are normalized so that the peak heights coincide). Since the Kondo scale $T_0 = 400$ K is much larger than the temperature, this measurement essentially probes the $T = 0$ lattice Kondo resonance below the Fermi level, convoluted with a Gaussian of width $\Delta E = 25$ meV. All other measurements in this low-temperature phase are for temperatures $T < T_v = 42$ K $\ll T_0 = 400$ K and can also be regarded as essentially zero-temperature measurements. At such low temperatures, the Kondo resonance is fully developed, so no temperature dependence is expected, and indeed almost none is seen [31].

Figure 14 shows reasonable agreement between the calculations and the experimental results. In particular, the theory reproduces the correct width of the near- E_F feature, as well as the slow decay of the intensity at negative energies. We attribute the latter to the non-Lorentzian decay of the Kondo resonance at high energies similar to that found for the impurity Kondo resonance [65] (whose lineshape for $|\omega| \gg T_0$ is of the Doniach-Sunjić type). The position of the peak in the intensity at $T \ll T_0$ is related to the position E_m of the Kondo resonance in $A(\omega, T)$. From Fig. 7 we estimate that $E_m(T \rightarrow 0)/T_0 \approx -0.5$ for the present calculations at $n_c = 0.4$. The experiments would indicate a value

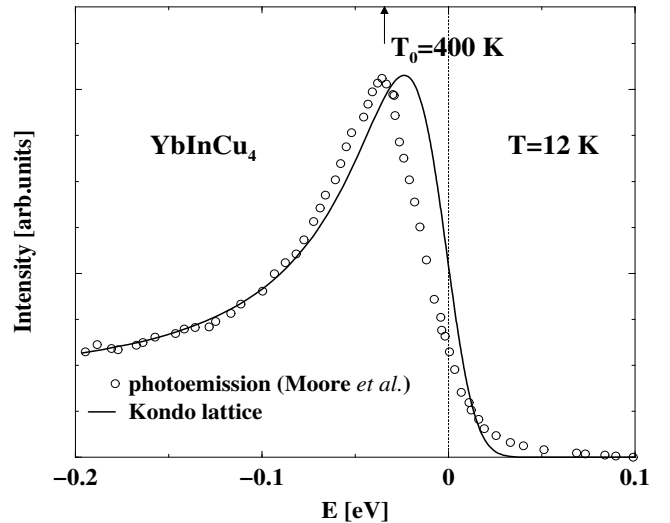


FIG. 14. Comparison of the calculated PES intensity for the lattice Kondo resonance with the experimentally measured intensity [31] for the $f^{7/2}$ near- E_F feature in YbInCu_4 at $T = 12$ K $\ll T_0 = 400$ K. The calculated curve includes the $\Delta E = 25$ meV Gaussian instrumental resolution.

closer to -1 , i.e. larger in magnitude than the $S = 1/2$ Kondo lattice model result. The predictions of the AIM in the Kondo regime (with occupancy ≈ 1) would be in far worse agreement, since from Fig. 8 we see that the Kondo resonance is pinned even more closely to the Fermi level than in the Kondo lattice calculations. It is important to note, however, that there is no fundamental relationship between E_m and the Kondo scale. E_m simply reflects a particle-hole asymmetry in the model, but on physical grounds one expects it to lie within approximately T_0 of the chemical potential. Its precise value, both for impurity and lattice models, depends on specific details influencing the particle-hole asymmetry, such as the ground-state degeneracy of the f state, the presence of low-lying crystal-field states, and the amount of mixed valence as reflected in the f -level occupancy (fixed to $n_f = 1$ in the Kondo lattice model) [66]. As our model describes a local ground-state doublet with $n_f = 1$, it would be surprising if it could capture the precise value of E_m/T_0 for YbInCu_4 , which would depend on such details. Hence the position of the peak in the intensity at $T \ll T_0$ is also not captured precisely. It is likely that a Kondo lattice model, including the f -orbital degeneracy, or the corresponding Anderson lattice model, will show complete agreement between theory and experiment.

B. High-temperature phase of YbInCu_4

We turn now to the high-temperature phase of YbInCu_4 , for which $T_0 = 30$ K and measurements have been taken up to 150 K $= 5 T_0$ [31]. This range of temperatures is interesting, because the results of the previ-

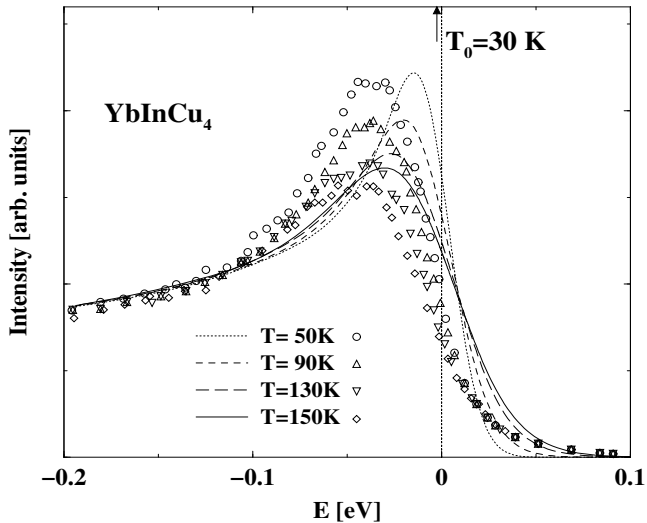


FIG. 15. Comparison of the temperature dependence of the calculated PES intensity for the lattice Kondo resonance with the experimentally measured intensity for YbInCu₄ [31]. The measurements were for the high-temperature phase, with a Kondo scale of $T_0 = 30$ K. We compare only with the $f^{7/2}$ near- E_F feature (the $f^{5/2}$ spin-orbit side band at -1.375 eV in the experiments is not included in the present model). The calculated curves are Gaussian convoluted to account for the instrumental and phonon broadening ΔE_{tot} of Eq. (9).

ous section predict a strong temperature dependence in the near- E_F spectra in the range $0 \leq T \leq 10 T_0$ due to the Kondo effect. A comparison of the measured intensities with the Kondo lattice model predictions is shown in Fig. 15. As in Fig. 14, the resolution and Kondo scales are taken from experiment and no attempt was made to obtain a best fit to the spectra by adjusting T_0 or ΔE . A phonon broadening reaching 50 meV at 150 K is included, as described above. This improves agreement for the two highest temperatures, but phonon broadening is not the main source of temperature dependence in the spectrum, which is instead the temperature dependence of the Kondo resonance in the spectral function $A(\omega, T)$. The experimental spectra are consistent with this interpretation, because they show a loss in intensity of the near- E_F feature as the temperature is increased from 50 K to 150 K: this agrees with the loss in spectral weight of the Kondo resonance with increasing temperature, and cannot be attributed to phonon broadening, which conserves the total spectral weight.

The lineshape is well reproduced by the calculations, as is the temperature dependence of the intensity. The curves are normalized so that the lowest-temperature peak heights in theory and experiment agree. This normalization gives agreement between theory and experiment for the tails and peak heights at all temperatures. Note, that at finite temperatures, the position of the intensity peak no longer reflects the Kondo resonance position (and therefore also not the Kondo scale). Thermal

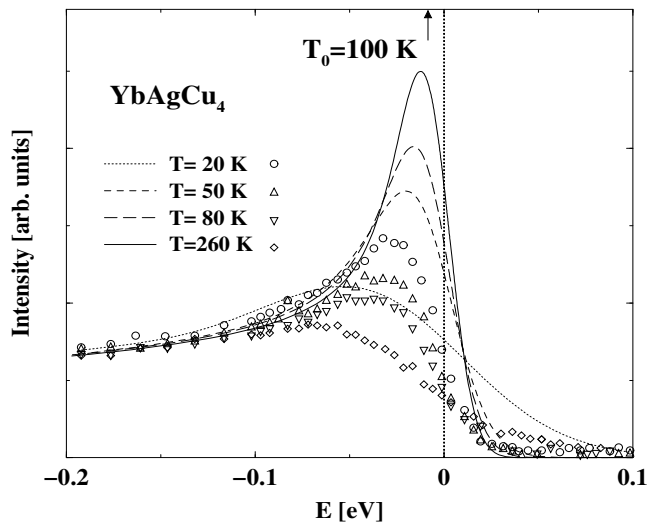


FIG. 16. Temperature dependence of the low energy PES intensity of YbAgCu₄ [23] compared to Kondo lattice calculations. Phonon broadening and instrumental resolution are accounted for as for YbInCu₄ in Fig. 15

broadening of the spectral function $A(\omega, T)$ in I_- , will shift the intensity peak to lower energies with increasing temperature, as observed in the calculations. The remaining discrepancy is essentially due to the oversimplified description of the f -states, resulting in too small a value for $E_m(T)$, as discussed above for the low temperature case.

C. YbAgCu₄

Figure 16 shows a comparison of the present calculations to early experimental results of Weibel *et al.* [23] for the temperature dependence of the near- E_F feature in YbAgCu₄. As for YbInCu₄, we take the experimental resolution and Kondo scale without any adjustment. The agreement is less good than for YbInCu₄, but still consistent with the interpretation of the temperature dependence of the spectrum as arising mainly from the Kondo effect. The discrepancy in the peak position has the same origin as that described above for YbInCu₄, and it could be overcome by a more realistic modeling of the f states of this compound.

For this compound, we normalize the curves to the tails in the intensity at negative energies. That part of the spectrum has much weaker temperature dependence, it reflects the non-Lorentzian tail of the Kondo resonance and it is the safest to use in case there are extrinsic (non-Kondo) temperature dependences close to E_F . In contrast to the case of YbInCu₄, we do not obtain agreement for both the tails and the peak height of the intensity as a function of temperature. We conclude that these early data, although indicating a Kondo effect in the temperature dependence of the spectrum close to the Fermi level,

are not fully consistent with our model. To investigate the origin of the discrepancy between theory and experiment, it would be interesting to repeat such experiments, particularly on single crystals as for YbInCu₄ [31].

VI. CONCLUSIONS

In summary, we have studied the temperature dependence of the single-particle spectral densities of the Kondo lattice model and their evolution with band filling within dynamical mean field theory. We found that the spectra exhibit two energy scales: a renormalized hybridization pseudogap scale T^* , which evolves from the true hybridization gap of the Kondo insulating state at $n_c = 1$ on moving away from half-filling, and a typically much smaller Fermi-liquid coherence scale T_0 , characterizing the formation of the main branch of the split lattice Kondo resonance at the Fermi level. The weight of the upper branch of this lattice Kondo resonance at $\omega \approx T^*$ becomes negligible for $n_c \lesssim 0.7$. The scale T^* was found to correlate with the single-ion Kondo scale. The high-temperature behavior of the local spectral densities is similar to that expected for a collection of independent Kondo impurities. We found that the lattice Kondo resonance develops over the same temperature range, $0 \leq T \lesssim 10T_0 < T^*$, as in the single-impurity models, at least for the range of band fillings studied in this paper: $0.4 \lesssim n_c \lesssim 0.9$. In this respect, the Kondo effect in this low-temperature phase, $T < T^*$, appears similar to the single-ion Kondo effect. However, the electrons involved have a strong f character arising from the renormalized bands formed below $T \approx T^*$. We interpret the above findings as indicating a two-stage Kondo effect for the formation of the paramagnetic heavy-fermion state: a single-ion Kondo effect at $T \gg T^*$, and a low-temperature Kondo effect at $T < T^*$ resulting from the modified electronic structure below T^* , and giving rise to the new scale T_0 .

The results for the temperature dependence of the lattice Kondo resonance were used to calculate the low-energy part of the f -level PES and IPES intensities of heavy-fermion systems. We made detailed predictions for the spectra of doped Kondo insulators ($n_c \lesssim 1$) and metallic heavy fermions. For the former, we found that most of the intensity of the Kondo resonance lies in the PES, and not in the IPES. This applies to hole-doped Ce or electron-doped Yb Kondo insulators. The predicted pseudogap in the f -electron spectrum is best seen in the PES of electron-doped Yb Kondo insulators. For hole-doped Ce systems, this would lie just above the Fermi level in the IPES spectrum. On moving away from the Kondo insulating toward the metallic heavy-fermion case, we found that the main intensity of the Kondo resonance shifts to the IPES spectrum and the PES and IPES intensities appear qualitatively similar to impurity-model

calculations.

We made a parameter-free comparison of our results with high-resolution PES data for YbInCu₄ and YbAgCu₄, taking the Kondo scales and resolution from the experiment. Good agreement was found for the lineshape and temperature dependence of YbInCu₄, although we argued that a more realistic treatment of the f -states (including, for example, orbital degeneracy) would be required to obtain the precise peak position in the PES intensity of the near- E_F feature. In the experimental spectra we found evidence of some phonon broadening at higher temperatures, but the main temperature dependence of the near- E_F spectrum is due to the Kondo effect.

The present study has focused attention on the paramagnetic metallic state of the $S = 1/2$ Kondo lattice model and has revealed some of the physics of this state, such as the relevant energy scales involved and how these appear in the PES and IPES spectra of heavy fermions. It would be interesting to identify these scales in other properties, such as in the optical conductivity, transport properties and in the thermodynamics. Work on this is in progress and will be reported elsewhere.

ACKNOWLEDGMENTS

We thank the Newton Institute - Cambridge and the ILL - Grenoble for support during the development of this project. NM also acknowledges support from the SISSA-Trieste and Italian INFM. We wish to thank Y. Baer, N. Brookes, D. Moore and S. J. Oh for useful discussions.

APPENDIX A: NRG AND DMFT DETAILS

We provide, here, some of the details of the NRG and the DMFT applied to the Kondo lattice model.

Starting from Eq.(3) we follow the standard procedure for casting the effective impurity model into a linear chain form suitable for an NRG calculation [34]. This first involves a logarithmic discretization of the conduction band about the chemical potential $\mu(T)$ (which for the purposes of this Appendix is taken as the zero of energy). The discretized energies are $\pm D_{\pm} \Lambda^{-n}$, $n = 0, 1, \dots$, where $\pm D_{\pm}$ are the upper (+) and lower (-) band edges, respectively, and $\Lambda > 1$ is the discretization parameter, set to 1.5 in the calculations. A unitary transformation of these states then yields a new tridiagonal set $b_{n,\sigma}$, $n = 0, 1, \dots$, such that $b_{0,\sigma} = c_{0,\sigma}$. The Hamiltonian takes the following form:

$$\mathcal{H}_{imp} = J \sum_{\mu,\nu} \mathbf{S} \cdot b_{0,\mu}^{\dagger} \sigma_{\mu,\nu} b_{0,\nu} + \sum_{n=0,\infty} \varepsilon_n b_{n,\nu}^{\dagger} b_{n,\nu} + \sum_{n=0,\infty} \lambda_n (b_{n,\nu}^{\dagger} b_{n+1,\nu} + H.c.). \quad (\text{A1})$$

We use this form for the actual calculations, which involve iteratively diagonalizing Eq. (A1) in the standard NRG manner [34], i.e. adding the orbitals $n = 0, 1, \dots$ successively and retaining only the lowest energy eigenstates at each stage. We retained 462 non-degenerate states at each NRG iteration and we checked that the spectra did not change significantly by further increasing the number of kept states. The spectra are calculated at the natural NRG temperature scales, $T_N \sim \lambda_N$ [67].

This NRG technique is the basic ingredient in the solution of the Kondo impurity problem at the core of the each DMFT step, then iterated to approach self consistency. We terminate the DMFT iteration when Eq. (4) is satisfied for ρ_c to an accuracy of 10^{-4} in the relative norm of successive iterates (i.e. $\|\rho_c^n - \rho_c^{n-1}\|/\|\rho_c^n\| < 10^{-4}$ where $\|\rho\| = \sqrt{\sum_i \rho(\omega_i)^2}$), and the chemical-potential self consistency is satisfied for n_c to at least 5 decimal places, for all fillings and temperatures.

For the case of a Bethe lattice, used in this paper, the self energy $\Sigma_\sigma(\omega, T)$ of Eq. (4) can be eliminated from the DMFT self consistency and left out of the calculation. However, it is required to calculate quantities such as transport coefficients, so we outline here its derivation. We first separate out the $n = 0$ conduction electron orbital and re-diagonalize the remaining orbitals, $n = 1, 2, \dots$, to obtain a new set of \mathbf{k} -states, $a_{\mathbf{k},\sigma}$, with dispersion $E_{\mathbf{k},\sigma}$. In terms of these, the effective impurity model becomes,

$$\begin{aligned} \mathcal{H}_{imp} = & J \sum_{\mu,\nu} \mathbf{S} \cdot \left(b_{0,\mu}^\dagger \boldsymbol{\sigma}_{\mu,\nu} b_{0,\nu} \right) + \sum_{\mu} \varepsilon_0 b_{0,\mu}^\dagger b_{0,\mu} \\ & + \sum_{\mathbf{k},\nu} E_{\mathbf{k},\nu} a_{\mathbf{k},\nu}^\dagger a_{\mathbf{k},\nu} + \sum_{\mathbf{k},\nu} \left(V_{\mathbf{k}} a_{\mathbf{k},\nu}^\dagger b_{0,\nu} + H.c. \right). \quad (\text{A2}) \end{aligned}$$

The hybridization matrix elements $V_{\mathbf{k}}$ are introduced formally via $\lambda_0 b_{1,\sigma} = \sum_{\mathbf{k}} V_{\mathbf{k}} a_{\mathbf{k},\sigma}$, which expresses $b_{1,\sigma}$ in terms of the new complete set of \mathbf{k} -states.

In order to obtain an expression for the self-energy, we follow the method in [68], and consider equations of motion for $G_{c,\sigma}(\omega, T) = \langle\langle c_{0,\sigma}; c_{0,\sigma}^\dagger \rangle\rangle \equiv \langle\langle b_{0,\sigma}; b_{0,\sigma}^\dagger \rangle\rangle$:

$$\begin{aligned} (\omega - \varepsilon_0) G_{c,\sigma}(\omega, T) &= 1 + \sum_{\mathbf{k}} V_{\mathbf{k}} \langle\langle a_{\mathbf{k},\sigma}; b_{0,\sigma}^\dagger \rangle\rangle + \Gamma_\sigma(\omega, T), \\ (\omega - E_{\mathbf{k},\sigma}) \langle\langle a_{\mathbf{k},\sigma}; b_{0,\sigma}^\dagger \rangle\rangle &= V_{\mathbf{k}} G_{c,\sigma}(\omega, T), \end{aligned}$$

where

$$\Gamma_\sigma(\omega, T) = \langle\langle O_\sigma; b_{0,\sigma}^\dagger \rangle\rangle, \quad (\text{A3})$$

and

$$O_\sigma = \frac{J}{2} (b_{0,-\sigma} S^{-\sigma} + \sigma b_{0,\sigma} S^z). \quad (\text{A4})$$

Solving the above equations for $G_{c,\sigma}(\omega, T)$ gives

$$G_{c,\sigma}(\omega, T) = [\omega - \varepsilon_0 - \Delta_\sigma(\omega, T) - \Sigma_\sigma(\omega, T)]^{-1} \quad (\text{A5})$$

$$\Delta_\sigma(\omega, T) = \sum_{\mathbf{k}} \frac{|V_{\mathbf{k}}|^2}{(\omega - E_{\mathbf{k}})} \quad (\text{A6})$$

$$\Sigma_\sigma(\omega, T) = \frac{\Gamma_\sigma(\omega, T)}{G_{c,\sigma}(\omega, T)}. \quad (\text{A7})$$

As discussed in Ref. [68], this form of the self-energy is best suited for DMFT(NRG) calculations. The hybridization function $\Delta_\sigma(\omega, T)$ includes the ‘‘single-particle’’ renormalization and broadening of the local Wannier orbital due to coupling to the remaining conduction electron orbitals $n = 1, 2, \dots$. It depends on temperature through the dependence of the parameters of the effective medium on temperature. The many-body renormalization and broadening of the local Wannier orbital is contained in the self energy. Σ_σ represents also the conduction-electron self energy of the correlated lattice model by the DMFT self-consistency condition (4): it vanishes in the non-interacting limit $J \rightarrow 0$. The DMFT self-consistency condition (4) reduces in the present case of a Bethe-lattice to

$$\varepsilon_0 + \Delta_\sigma(\omega, T) = \frac{D^2}{4} G_{c,\sigma}(\omega, T). \quad (\text{A8})$$

APPENDIX B: SPECTRAL FUNCTIONS

The low-energy part of the f -electron PES of the Kondo lattice model (1) is determined from the local T-matrix, \mathcal{T}_0 , of (1), via

$$A(\omega, T) = -\frac{1}{\pi} \text{Im } \mathcal{T}_0(\omega, T), \quad (\text{B1})$$

and \mathcal{T}_0 is related to the \mathbf{k} -dependent T-matrix of the Kondo lattice model $\mathcal{T}_{\mathbf{k},\mathbf{k}'}$, via

$$\mathcal{T}_0(\omega, T) = \sum_{\mathbf{k},\mathbf{k}'} \mathcal{T}_{\mathbf{k},\mathbf{k}'}(\omega, T). \quad (\text{B2})$$

$\mathcal{T}_{\mathbf{k},\mathbf{k}'}$ is defined by the identity

$$G_c^{\mathbf{k},\mathbf{k}'} = \delta_{\mathbf{k},\mathbf{k}'} G_0^{\mathbf{k}\mathbf{k}} + G_0^{\mathbf{k}\mathbf{k}} \mathcal{T}_{\mathbf{k},\mathbf{k}'} G_0^{\mathbf{k}'\mathbf{k}'}. \quad (\text{B3})$$

where $G_0^{\mathbf{k}\mathbf{k}}$ and $G_c^{\mathbf{k}\mathbf{k}}$ are, respectively, the non-interacting and interacting conduction electron Green’s functions of the Kondo lattice model. An explicit expression for \mathcal{T}_0 has been given in Ref. [69]: $\mathcal{T}_0 = \langle\langle O_\sigma; O_\sigma^\dagger \rangle\rangle$, where the operator O_σ is defined in Eq. A4. Note that $A(\omega, T)$ only describes the part of the f -spectrum lying close to the Fermi level and associated with the lattice Kondo resonance. The higher-energy f -electron excitations associated with the f -level satellite peaks are projected out in this model. Hence, unlike ρ_c , $A(\omega, T)$ is not normalized to unity. Its integrated weight reflects the weight

of the many-body Kondo resonance and will therefore depend strongly on temperature. Finally, for the purposes of identifying the relevant low-energy scales, it is also useful to consider the local magnetic excitation spectrum, $\chi''_{zz}(\omega, T)$, of the effective quantum impurity model (3). This is defined by

$$\chi''_{zz}(\omega, T) = -\frac{1}{\pi} \text{Im} \chi_{zz}(\omega, T), \quad (\text{B4})$$

where $\chi_{zz}(\omega, T)$ is the longitudinal dynamical susceptibility of (3) after self-consistency is achieved.

-
- [1] Y. Kuramoto, and Y. Kitaoka, *Dynamics of Heavy Electrons* (Oxford University Press, Oxford, England, 2000).
- [2] A. C. Hewson, *The Kondo Problem to Heavy Fermions* (Cambridge University Press, Cambridge, England 1993).
- [3] N. Grewe, and F. Steglich, in *Handbook of the Physics and Chemistry of Rare Earths*, Vol. 14, edited by K. A. Gschneider Jr., and L. Eyring (North Holland, Amsterdam, 1991), p. 343.
- [4] P. Wachter, in *Handbook of the Physics and Chemistry of Rare Earths*, Vol. 19, edited by K. A. Gschneider Jr., L. Eyring, G. H. Lander and G. R. Choppin (North Holland, Amsterdam, 1994), p. 177.
- [5] P. A. Lee, T. M. Rice, J. W. Serene, L. J. Sham, and J. W. Wilkins, *Comments in Condens. Matt. Phys.* **12**, 99 (1986).
- [6] G. R. Stewart, *Rev. Mod. Phys.* **56**, 755 (1984).
- [7] H. Tsunetsugu, M. Sigrist, and K. Ueda, *Rev. Mod. Phys.* **69**, 809 (1997).
- [8] N. Shibata and K. Ueda, *J. Phys. Cond. Matt.* **11**, R1 (1999); N. Shibata, in *Density Matrix Renormalization*, edited by I. Peschel, X. Wang, M. Kaulke, and K. Hallberg (Springer, Berlin, Germany 1999).
- [9] P. Fazekas, *Lecture Notes on Electron Correlation and Magnetism*, Vol. 5, in Series in Modern Condensed Matter Physics (World Scientific, Singapore, 1999).
- [10] W. Metzner and D. Vollhardt, *Phys. Rev. Lett.* **62**, 324 (1989).
- [11] E. Müller-Hartmann, *Z. Phys. B* **74**, 507 (1989).
- [12] F. J. Ohkawa, *J. Phys. Soc. Japan* **60**, 3218 (1991); *Prog. Theor. Phys. (Suppl.)* **106**, 95 (1991).
- [13] A. Georges and G. Kotliar, *Phys. Rev. B* **45**, 6479 (1992).
- [14] M. Jarrell, *Phys. Rev. Lett.* **69**, 168 (1992).
- [15] A. Georges, G. Kotliar, W. Krauth, and M. Rozenberg, *Rev. Mod. Phys.* **68**, 13 (1996).
- [16] J. W. Allen, G.-H. Gweon, H. T. Schek, L.-Z. Liu, L. H. Tjeng, J.-H. Park, W. P. Ellis, C. T. Chen, O. Gunnarsson, O. Jepsen, O. K. Andersen, Y. Dalichaouch, and M. B. Maple, *J. App. Phys.* **87**, 6088 (2000).
- [17] A. J. Arko, P. S. Riseborough, A. B. Andrews, J. J. Joyce, A. N. Tahvildar-Zadeh, and M. Jarrell, in *Handbook of the Physics and Chemistry of Rare Earths*, Vol. **26**, edited by K. A. Gschneider Jr., and L. Eyring (North Holland, Amsterdam, 1999), p. 265.
- [18] D. Malterre, M. Gioni, and Y. Baer, *Adv. in Physics* **45**, 299 (1996).
- [19] J. W. Allen, S. J. Oh, O. Gunnarsson, K. Schönhammer, M. B. Maple, M. S. Torikachvili, and I. Lindau, *Adv. in Physics* **35**, 275 (1986).
- [20] O. Gunnarsson and K. Schönhammer, *Phys. Rev. B* **28**, 4315 (1983).
- [21] N. E. Bickers, D. L. Cox, and J. W. Wilkins, *Phys. Rev. B* **36**, 2036 (1987).
- [22] F. Patthey, J. M. Imer, W. D. Schneider, H. Beck, Y. Baer, and B. Delley, *Phys. Rev. B* **42**, 8864 (1990).
- [23] P. Weibel, M. Gioni, D. Malterre, B. Dardel, Y. Baer, and M. J. Besnus, *Z. Phys. B* **91**, 337 (1993).
- [24] L. H. Tjeng, S.-J. Oh, E.-J. Cho, H.-J. Lin, C. T. Chen, G.-H. Gweon, J.-H. Park, J. W. Allen, T. Suzuki, M. S. Makivic, and D. L. Cox, *Phys. Rev. Lett.* **71**, 1419 (1993).
- [25] M. Garnier, K. Breuer, D. Purdie, M. Hengsberger, and Y. Baer, *Phys. Rev. Lett.* **78**, 4127 (1987).
- [26] J. J. Joyce, A. J. Arko, J. Lawrence, P. C. Canfield, R. J. Bartlett, J. D. Thompson, *Phys. Rev. Lett.* **68**, 236 (1992).
- [27] R. I. R. Blyth, J. J. Joyce, A. J. Arko, P. C. Canfield, A. B. Andrews, Z. Fisk, J. D. Thompson, R. J. Bartlett, P. Riseborough, J. Tang, and J. Lawrence, *Phys. Rev. B* **48**, 9497 (1993).
- [28] F. Reinert, R. Claessen, G. Nicolay, D. Ehm, S. Hüfner, W. P. Ellis, G.-H. Gweon, J. W. Allen, B. Kindler, and W. Assmus, *Phys. Rev. B* **58**, 12808 (1998).
- [29] J. J. Joyce, A. J. Arko, L. A. Morales, J. L. Sarrao, and H. Höchst, *Phys. Rev. B* **63**, 197101 (2001).
- [30] F. Reinert, R. Claessen, G. Nicolay, D. Ehm, S. Hüfner, W. P. Ellis, G.-H. Gweon, J. W. Allen, B. Kindler, and W. Assmus, *Phys. Rev. B* **63**, 197102 (2001).
- [31] D. P. Moore, J. J. Joyce, A. J. Arko, J. L. Sarrao, L. Morales, H. Hochst, Y. D. Chuang, *Phys. Rev. B* **62**, 16492 (2000).
- [32] J. D. Denlinger, G.-H. Gweon, J. W. Allen, and J. L. Sarrao, *cond-mat/0107357*.
- [33] A. Georges, G. Kotliar, and Q. Si, *Int. J. of Mod. Phys. B* **6**, 705 (1992).
- [34] K. G. Wilson, *Rev. Mod. Phys.* **47**, 773 (1975); H. R. Krishnamurthy, J. W. Wilkins, and K. G. Wilson, *Phys. Rev. B* **21**, 1003 (1980).
- [35] T. A. Costi and A. C. Hewson, *Phil. Mag. B* **65**, 1165 (1992); T. A. Costi, A. C. Hewson, and V. Zlatić, *J. Phys. Cond. Matt.* **6**, 2519 (1994).
- [36] W. Hofstetter, *Phys. Rev. Lett.* **85**, 1508 (2000). This refinement reduces finite-size errors in NRG spectra. It is important for finite magnetic fields. It does not improve significantly the zero-field spectra reported in this paper.
- [37] R. Bulla, T. A. Costi, and D. Vollhardt, *Phys. Rev. B* **64**, 045103 (2001).
- [38] G. Aeppli and Z. Fisk, *Comments in Condens. Matt. Phys.* **16**, 155 (1992).
- [39] M. F. Hundley *et al.*, *Phys. Rev. B* **42**, 6842 (1990); *ibid.*, **50**, 18142 (1994).
- [40] F. Iga, M. Kasaya, and T. Kasuya, *J. Magn. Magn. Mater.* **52**, 279 (1985).

- [41] Z. Fisk, P. C. Canfield, W. P. Beyermann, J. D. Thompson, M. F. Hundley, H. R. Ott, E. Felder, M. B. Maple, M. A. Lopez de la Torre, P. Visani, and C. L. Seaman, Phys. Rev. Lett. **67**, 3310 (1991).
- [42] R. M. Martin, Phys. Rev. Lett. **48**, 362 (1982).
- [43] H. Kaga and H. Kubo, Solid State Commun. **65**, 267 (1987).
- [44] For the values of the band filling used in our calculations we find $T_0(n_c = 0.9) = 1.46 \times 10^{-3}D$, $T_0(n_c = 0.8) = 9.26 \times 10^{-4}D$, $T_0(n_c = 0.7) = 5.33 \times 10^{-4}D$, and $T_0(n_c = 0.4) = 9.63 \times 10^{-5}D$.
- [45] Th. Pruschke, R. Bulla, and M. Jarrell, Phys. Rev. B **61**, 12808 (1999).
- [46] S. Burdin, A. Georges, and D. R. Grempel, Phys. Rev. Lett. **85**, 1048 (2000).
- [47] M. Jarrell, Phys. Rev. B **51**, 7429 (1995).
- [48] T. E. Mason, G. Aepli, A. P. Ramirez, K. N. Clausen, C. Broholm, N. Stückeli, E. Bücher, and T. T. M. Palstra, Phys. Rev. Lett. **69**, 490 (1992).
- [49] A. Severing, J. D. Thompson, P. C. Canfield, Z. Fisk and P. Riseborough, Phys. Rev. B **44**, 6832 (1991).
- [50] A. N. Tahvildar-Zadeh, M. Jarrell, and J. K. Freericks, Phys. Rev. B **55**, 3332 (1997).
- [51] A. N. Tahvildar-Zadeh, M. Jarrell, and J. K. Freericks, Phys. Rev. Lett. **80**, 5168 (1998).
- [52] P. Nozières, Ann. Phys. Fr. **10**, 19 (1985); P. Nozières, Eur. Phys. J. B **6**, 447 (1998).
- [53] J. M. Lawrence, P. S. Riseborough, C. H. Booth, J. L. Sarrao, J. D. Thompson, and R. Osborn, Phys. Rev. B **63**, 054427 (2001); J. M. Lawrence, T. Ebihara, P. S. Riseborough, C. H. Booth, M. F. Hundley, P. G. Pagliuso, J. L. Sarrao, J. D. Thompson, M. H. Jung, A. H. Lacerda, and G. H. Kwei, cond-mat/0107638.
- [54] K. Breuer, S. Messerli, D. Purdie, M. Garnier, M. Hengsberger, G. Panaccione, Y. Baer, T. Takahashi, S. Yoshii, M. Kasaya, K. Katoh, and T. Takabatake, Europhys. Lett. **41**, 565 (1998).
- [55] H. Kumigashira, T. Takahashi, S. Yoshii, and M. Kasaya, Phys. Rev. Lett. **87**, 067206 (2001).
- [56] M. J. Rozenberg, G. Kotliar and H. Kajueter, Phys. Rev. B **54**, 8452 (1996).
- [57] T. Susaki, T. Konishi, A. Sekiyama, T. Mizokawa, A. Fujimori, T. Iwasaki, S. Ueda, T. Matsushita, S. Suga, H. Ishii, F. Iga, and M. Kasaya, Phys. Rev. B **56**, 13727 (1997).
- [58] E. A. Goremychkin and R. Osborn, Phys. Rev. B **47**, 14280 (1993).
- [59] F. Reinert, D. Ehm, S. Schmidt, G. Nicolay, S. Hüfner, J. Kroha, O. Trovarelli, and C. Geibel, Phys. Rev. Lett. **87**, 106401 (2001).
- [60] J. M. Lawrence, R. Osborn, J. L. Sarrao and Z. Fisk, Phys. Rev. B **59**, 1134 (1997); J. M. Lawrence, S. M. Shapiro, J. L. Sarrao and Z. Fisk, Phys. Rev. B **55**, 14467 (1999).
- [61] A. Severing, E. Gratz, B. D. Rainford, and K. Yoshimura, Physica B **163**, 409 (1990); A. Severing, A. P. Murani, J. D. Thompson, Z. Fisk, and C.-K. Loong, Phys. Rev. B **41**, 1739 (1990).
- [62] J. L. Sarrao, C. D. Immer, C. L. Benton, Z. Fisk, J. M. Lawrence, D. Mandrus, and J. D. Thompson, Phys. Rev. B **54**, 12207 (1996).
- [63] C. Rossel, K. N. Yang, M. B. Maple, Z. Fisk, E. Zirngiebel, and J. D. Thompson, Phys. Rev. B **35**, 1914 (1987).
- [64] M. J. Besnus, P. Haen, N. Hamdaoui, A. Herr and A. Meyer, Physica B **163**, 571 (1990).
- [65] H. O. Frota and L. N. Oliveira, Phys. Rev. B **43**, 7871 (1986).
- [66] PES from Ref. [31] suggest an f -hole count of $14 - n_f = 0.6$ in the low-temperature phase, and $14 - n_f = 0.7$ in the high-temperature phase of YbInCu₄, indicating a degree of mixed-valence character. L₃ x-ray absorption measurements [70] estimate $14 - n_f \approx 0.96$ for $T > T_v$ and $14 - n_f \approx 0.85$ for $T < T_v$, i.e. well within the Kondo regime.
- [67] This natural sequence of temperatures are used for Figs. 7, 10-13. Spectra for intermediate temperatures, as in Figs. 15-16, are obtained by interpolation.
- [68] R. Bulla, A. C. Hewson, and Th. Pruschke, J. Phys. Cond. Matt. **10**, 8365 (1998).
- [69] T. A. Costi, Phys. Rev. Lett. **85**, 1504 (2000).
- [70] A. L. Cornelius, J. M. Lawrence, J. L. Sarrao, Z. Fisk, M. F. Hundley, G. H. Kwei, J. D. Thompson, C. H. Booth, and F. Bridges, Phys. Rev. B **56**, 7993 (1987).